ELSEVIER

Materials Science and Engineering B63 (1999) 88–95

MATERIALS SCIENCE & ENGINEERING B

www.elsevier.com/locate/mseb

Metal–insulator transition and magnetotransport in III–V compound diluted magnetic semiconductors

Y. Iye [a,b,*], A. Oiwa [a], A. Endo [a], S. Katsumoto [a,b], F. Matsukura [c], A. Shen [c], H. Ohno [c], H. Munekata [d]

[a] *Institute for Solid State Physics, University of Tokyo, Roppongi, Minato-ku, Tokyo 106-8666, Japan*
[b] *Core Research for Evolutionary Science and Technology (CREST), Japan Corporation of Science and Technology, Mejiro, Toshima-ku, Tokyo 171-0031, Japan*
[c] *Research Institute for Electrical Communication, Tohoku University, Katahira, Aoba-ku, Sendai 980-8577, Japan*
[d] *Imaging Science and Engineering Laboratory, Tokyo Institute of Technology, Nagatsuda, Midori-ku, Yokohama 226-8503, Japan*

Abstract

Structural, magnetic and transport properties of diluted magnetic semiconductors, (Ga, Mn)As and (In, Mn)As, have been investigated. Manganese can be substitutionally doped into the group III site of the zincblend structure up to several percent. With Mn content of a few percent, these systems exhibit ferromagnetism at low temperatures. The highest Curie temperature so far achieved is ~ 100 K for (Ga, Mn)As. The saturated magnetization values are consistent with $S = 5/2$ local moment, suggesting divalent Mn which acts as an acceptor. The system becomes metallic with increasing Mn content, but a further increase of Mn content tends to decrease the hole density and increase disorder so that the system becomes nonmetallic again at higher Mn concentrations. Large negative magnetoresistance and highly anisotropic transport are observed in the semiconducting samples at low temperatures. The magnetic anisotropy in ultrathin films is found to be strongly affected by the lattice-mismatch-induced strain.

Keywords: Diluted magnetic semiconductor; Carrier-induced ferromagnetism; Anomalous Hall effect; Negative magnetoresistance; Metal–insulator transition; Lattice-mismatch-induced strain

1. Introduction

Although semiconductors and magnetic materials constitute the basis of modern electronics, their basic research have been developed with relatively little interdisciplinary communications. Magnetic semiconductors constitute a unique class of materials in which the two disciplines are intertwined. Much work has been conducted on diluted magnetic semiconductors (DMS) based on II–VI compounds such as (Cd, Mn)Te and (Zn, Mn)Se [1]. Diluted magnetic semiconductors based on III–V compounds constitute a relatively new class of materials that demonstrate many interesting phenomena where transport and magnetism are intimately correlated. Since GaAs and other III–V compounds are the key materials for the modern opto-electronics, one may expect the III–V compound diluted magnetic semiconductors to open the future of opto-magneto-electronics.

Unlike the II–VI compounds, the III–V compounds have been found difficult to dope with Mn. For example, bulk crystals of (Ga, Mn)As have been prepared with Mn content only up to a few tenths of a percent. With the advent of off-equilibrium crystal growth technique by molecular beam epitaxy, samples of $Ga_{1-x}Mn_xAs$ and $In_{1-x}Mn_xAs$ with Mn content high enough for interesting magnetic activities have become available. This research area is still in its infancy, and there is a growing accumulation of experimental data that awaits a unified picture. In this paper, we describe some of the basic properties of these systems and discuss spin-dependent transport phenomena.

* Corresponding author. Tel.: +81-03-34780536; fax: +81-03-34780536.
E-mail address: iye@issp.u-tokyo.ac.jp (Y. Iye)

0921-5107/99/$ - see front matter
PII: S0921-5107(99)00057-4

2. Crystal structure and growth

The stable crystal structure of MnAs is NiAs-type, which differs from the zincblend structure of GaAs and InAs. Manganese atoms introduced in GaAs or InAs tend to segregate to form MnAs. This severely limits the Mn solubility in the equilibrium condition, and makes Mn doping into GaAs and InAs difficult. Munekata et al. [2] were first to succeed in epitaxial growth of $In_{1-x}Mn_xAs$ with Mn content up to a few percent by off-equilibrium molecular beam epitaxy at low substrate temperatures. Fig. 1 is a diagram showing various phases of the MBE grown $In_{1-x}Mn_xAs$, that occur depending on the Mn content x and the substrate temperature T_{sub} [3]. It has been found that for the same Mn content, the carrier density varies widely depending on the substrate temperature, and even the carrier type (p or n) changes. For the reason to be described below, we are mostly interested in the p-type samples. $In_{1-x}Mn_xAs$, thick films were grown typically at substrate temperature $T_{sub} \approx 300$°C directly on GaAs(100) substrate with Mn content x up to $x \approx 0.03$. Use of (Al, Ga)Sb as a buffer layer has proved to relax the constraint for the growth of $In_{1-x}Mn_xAs$ layer. For (In, Mn)As/(Al, Ga)Sb system, p-$In_{1-x}Mn_xAs$ can be grown with substrate temperature as low as $T_{sub} \approx$ 170°C and with Mn content in excess of $x \approx 0.1$.

Growth of $Ga_{1-x}Mn_xAs$ was more recently achieved at substrate temperatures of $\sim T_{sub} \approx 250$°C by Ohno et al.[4]. Under properly chosen growth conditions, homogeneous $Ga_{1-x}Mn_xAs$ thick films up to $\sim x \approx$ 0.07 have been prepared. Surface segregation of Mn atoms and the formation of MnAs phase becomes discernible at higher Mn contents.

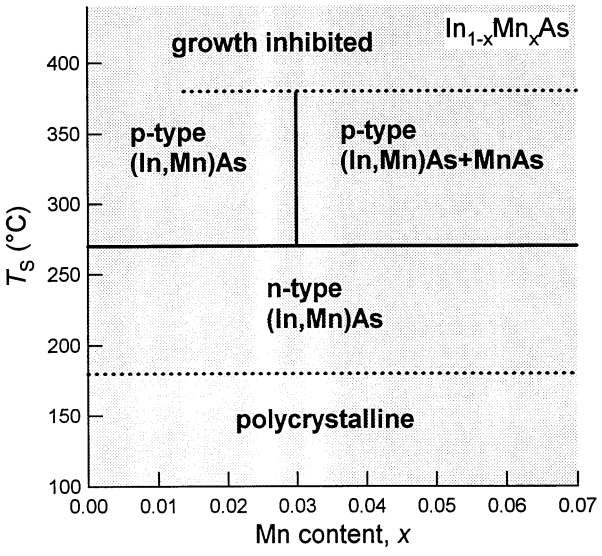

Fig. 1. Various phases of $In_{1-x}Mn_xAs$ occurring under different MBE growth conditions [2].

Manganese atoms substitutionally enter the group III atom site of the zincblend structure. X-ray diffraction studies show that the lattice constant of the zincblend structure increases with x for $Ga_{1-x}Mn_xAs$ and decreases slightly for $In_{1-x}Mn_xAs$. For the range of successful growth, the lattice constant changes linearly with x. The linear extrapolations of the x-dependence of the lattice constant for $Ga_{1-x}Mn_xAs$ and $In_{1-x}Mn_xAs$ roughly coincide at $x = 1$. This value at $x = 1$ corresponds to the lattice constant of a hypothetical zincblend MnAs. Further evidence in support of substitutional Mn occupancy of the group III atom site of the zincblend structure has been furnished by the extended X-ray absorption fine structure (EXAFS) experiment [5,6].

Since these materials are grown as epitaxial film, it is expected that the underlying substrate has a deep influence on their properties. $Ga_{1-x}Mn_xAs$ is usually grown on GaAs substrate. GaAs exerts a compressive stress to the epitaxial $Ga_{1-x}Mn_xAs$ layer. For the growth of $In_{1-x}Mn_xAs$ on GaAs substrate, GaSb is often used as a buffer layer. The GaSb underlayer exerts a tensile stress to the epitaxial $In_{1-x}Mn_xAs$ layer. Use of AlSb underlayer increases the tensile stress.

3. Doping and carrier-induced ferromagnetism

What makes these III–V compounds DMS most attractive is the ferromagnetism they exhibit above the critical values of Mn content. As shown below, the ferromagnetism in these materials is intimately linked with the presence of mobile carriers (holes). Fig. 2(a) shows the temperature dependence of resistivity for 150 nm thick films of $Ga_{1-x}Mn_xAs$ grown on GaAs substrate [7]. In the low x range, the hole density is proportional to x. The temperature dependence of the resistivity for the $x = 0.015$ sample can be fitted to an activation type with activation energy $\Delta \approx 75$ meV which may be compared with a reported value ≈ 110 meV for an isolated Mn acceptor in GaAs [8]. The system undergoes a insulator-metal transition at $\sim x \approx$ 0.03. The $x = 0.035$ sample shows metallic temperature dependence of resistivity. The broad hump of resistivity is seen at around the ferromagnetic transition temperature $T_C \approx 60$ K. The $x = 0.043$ sample is also metallic but the resistivity is higher than the $x = 0.035$ sample despite of the larger nominal acceptor density. For still higher x the system reenters the nonmetallic state. It appears that for the Mn content in excess of ~ 0.04, the mobile hole density no longer increases with increasing x but even decreases.

It is worth pointing out in passing that the presently found critical Mn concentration for the insulator–metal transition $x \approx 0.03$ is more than an order of

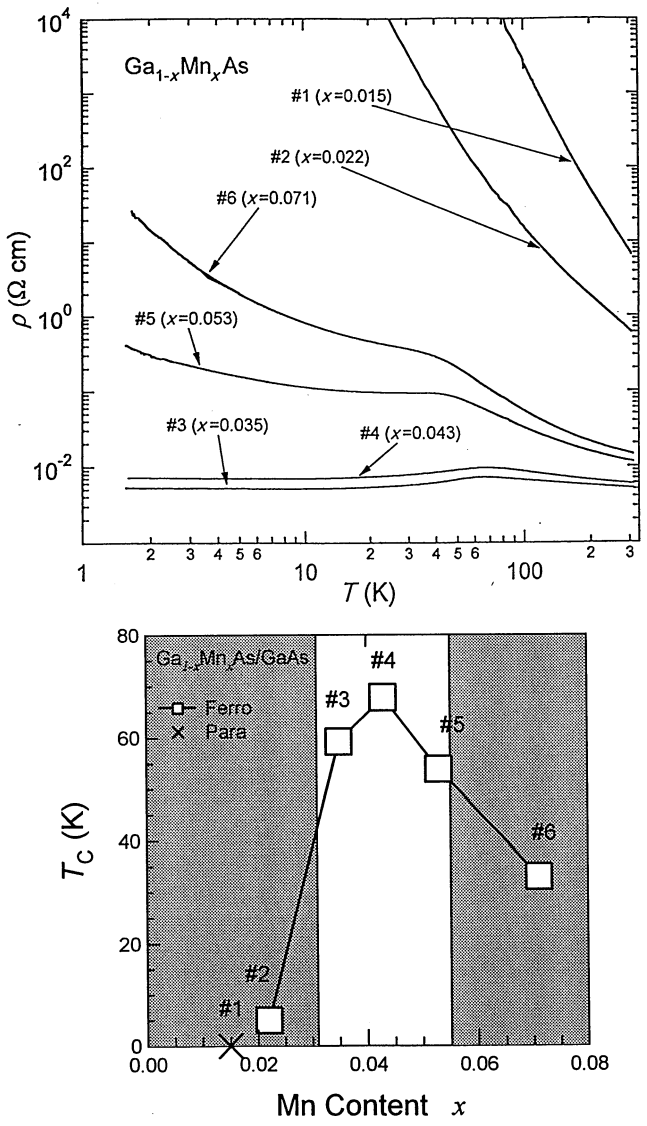

Fig. 2. (a)Temperature dependence of resistivity in 150 nm thick films of $Ga_{1-x}Mn_xAs$ with different values of x; (b) The Curie temperature as a function of the Mn content x. The shaded regions are non-metallic phases.

magnitude higher than the value reported earlier for bulk crystal [9]. The latter value is claimed to be in agreement with the Mott's criterion $a_B^* N_C \approx 0.25$. However, the 'metallic' samples in [8] are not really metallic. Thus, the critical hole density for the insulator–metal transition for $Ga_{1-x}Mn_xAs$ is significantly higher than the estimate based on the Mott's criterion assuming hydrogenic impurity state at the acceptor site.

The Curie temperature T_C was determined by measuring the temperature dependence of magnetization and making an Arrott plot. The broad hump in the resistivity such as seen in Fig. 2(a) serves as indicator of T_C. Fig. 2(b) shows T_C as a function of x. The Curie temperature increases with increasing x but saturates at higher x and eventually decreases. The maximum T_C so far achieved in $Ga_{1-x}Mn_xAs$ is $T_C \approx 100$ K. Fig. 3 shows similar data for 1200 nm thick films of $In_{1-x}Mn_xAs$. The overall trend of conduction and magnetism as a function of Mn content is similar to $Ga_{1-x}Mn_xAs$. However, unlike the latter $In_{1-x}Mn_xAs$ becomes barely metallic even in the optimum range of x. The Curie temperatures for $In_{1-x}Mn_xAs$ thick films do not exceed 10 K thus far. On the other hand, ferromagnetic transition at $T_C \approx 35$ K has been achieved in $In_{1-x}Mn_xAs$/(Ga, Al)Sb heterostructures [10].

It has been established that the occurrence of ferromagnetism is closely linked to the presence of hole carriers. It has been demonstrated that ferromagnetism of $Ga_{1-x}Mn_xAs$ disappears when it is made n-type by doping with Sn [11]. Similar behavior has been reported earlier for the $In_{1-x}Mn_xAs$ system [12]. The notion of

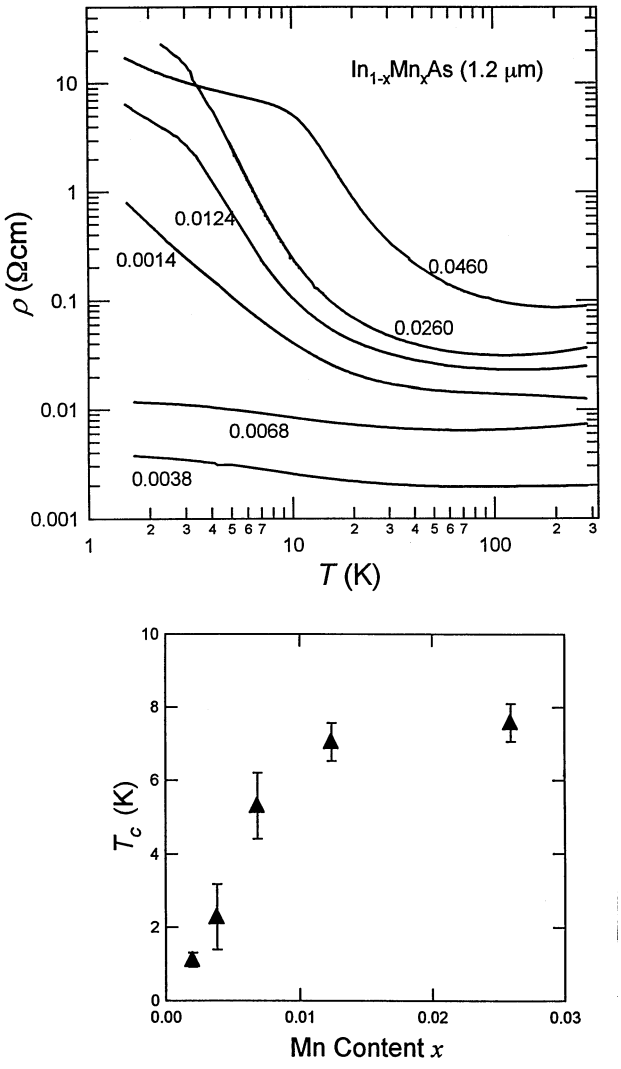

Fig. 3. (a) Temperature dependence of resistivity in 1200 nm thick films of $In_{1-x}Mn_xAs$ with different values of x; (b)The Curie temperature as a function of the Mn content x.

carrier-mediated ferromagnetism leads to attempts to control magnetism by external manipulation of carrier density by light irradiation or gate electrode. Ferromagnetism induced by persistent photocarriers is reported for a $In_{0.94}Mn_{0.06}As/GaSb$ system on the verge of ferromagnetic transition [13].

The basic mechanism for the carrier-induced ferromagnetism is currently debated. The ferromagnetic interaction must be fairly long-ranged. One line of thought invokes an analogue of Ruderman–Kittel–Kasuya–Yosida (RKKY) interaction between localized Mn moments mediated by the hole gas [14]. In comparison to metallic systems with dilute magnetic imputies, the Fermi wavenumber is much smaller so that the ferromagnetic range is expected to extend much longer than the usual metallic case. Another line of thought emphasizes the *d*-character of the holes and attribute the ferromagnetic interaction to a kind of double exchange mechanism based on a strong Hund coupling at the Mn site [15]. Which of these approaches is more appropriate is not clear at the moment. The key factor is to what extent the carriers (As *p*-holes) have the Mn *d*-hole character.

Study of pressure effects may furnish some clue for discriminating the two mechanisms. The change in T_C with pressure however is a total outcome of various pressure-dependent factors which are not easy to disentangle. We have studied the pressure effect on T_C in the $Ga_{1-x}Mn_xAs$ ($x = 0.035$) sample and have found $d \ln T_C/dp \approx -0.04 \pm 0.01$ GPa^{-1} [16]. We expect the p–d exchange coupling to increase with pressure as $J_{pd} \propto d^{-7/2}$ d being the Mn-As distance. The observed pressure coefficient of T_C is considerably smaller than the estimated change in J_{pd}.

On the other hand the Hall measurement under pressure seems to indicate some decrease of hole density with pressure. (With the ambiguity associated with the difficulty of carrier density estimation from the Hall data in this system.) It appears that the observed small pressure dependence of T_C is due to partial cancellation of these two major factors.

4. Magnetic properties

Fig. 4 shows magnetization curves at 2 K for the six samples of $Ga_{1-x}Mn_xAs$ [7]. The high field limit values of magnetization roughly agree with the calculated saturation magnetization assuming $S = 5/2$ (Mn^{2+}) local moments, although there is experimental uncertainty associated with the error in the determination of x. The ferromagnetic hysteresis loop occurs in the low field range $B < 0.1$ T, which is not visible in the scale of this Fig.. For samples with larger x, the amplitude of the low field hysteresis loop is significantly smaller than the saturation magnetization. This indicates that not all

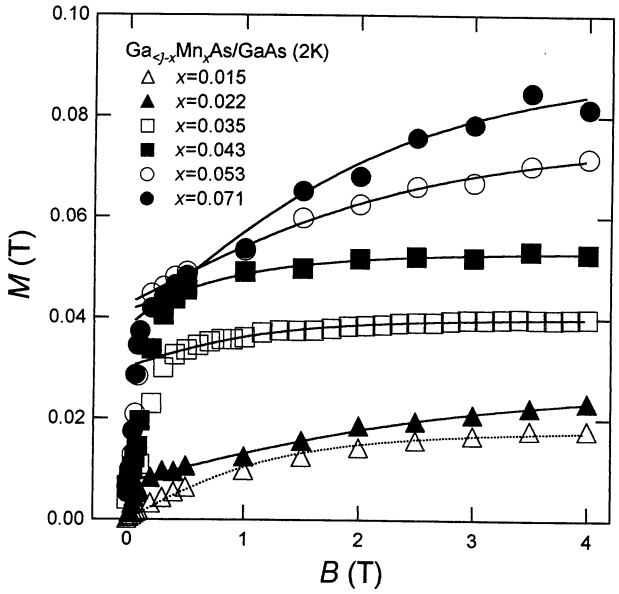

Fig. 4. Magnetization curves at 2 K for the same samples of $Ga_{1-x}Mn_xAs$ as for Fig. 2.

the Mn moments participate in the low field hysteresis loop, and there is a significant fraction of the Mn moments that takes much higher field to be fully aligned.

For the detection of ferromagnetism in these materials, the anomalous Hall effect is conveniently used as a 'built-in' magnetometer. This is particularly useful for ultrathin film samples for which direct magnetization measurement is difficult even with a sensitive SQUID magnetometer. Fig. 5 shows the Hall resistance at 4.2 K in ultrathin film samples of $In_{1-x}Mn_xAs$ grown on GaSb and AlSb buffer layers [17]. The relevant parameters are given in Table 1.

The Hall resistance in a magnetic substance can be expressed as

$$\rho_H = \frac{R_0}{d} B + \frac{R_s}{d} M, \quad (1)$$

where d is the thickness of the film, R_0 is the normal (ordinary) Hall coefficient associated with the Lorentz force proportional to the magnetic field B, end R_s represents the so-called anomalous (extraordinary) Hall coefficient proportional to the magnetization M. Traces shown in Fig. 5 are dominated by the anomalous Hall term, so that they reflect the M versus B curves and exhibit ferromagnetic hysteresis at this temperature.

The three hysteresis loops in Fig. 5 differ in shape and in coercive field. Sample 1 behaves as a soft magnet, while samples 2 and 3 are harder. Fig. 6 shows the Hall resistance in samples 1 and 2 for different angles of the external magnetic field with respect to the plane normal. In the case of sample 1 (Fig. 6(a)), the data collapse to a single curve by taking $\rho_H/\cos\theta$ as the

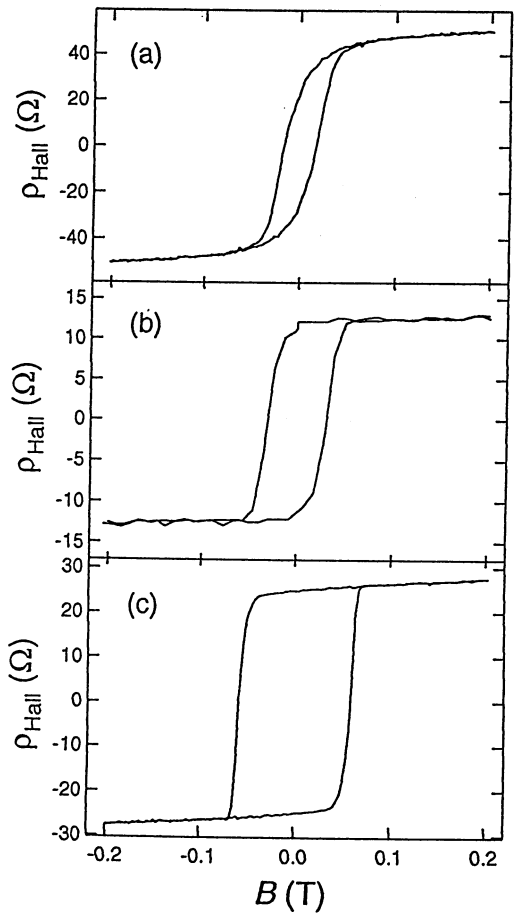

Fig. 5. Hall resistance of ultrathin $In_{1-x}Mn_xAs$ films listed in Table 1 at 4.2 K showing ferromagnetic hysteresis.

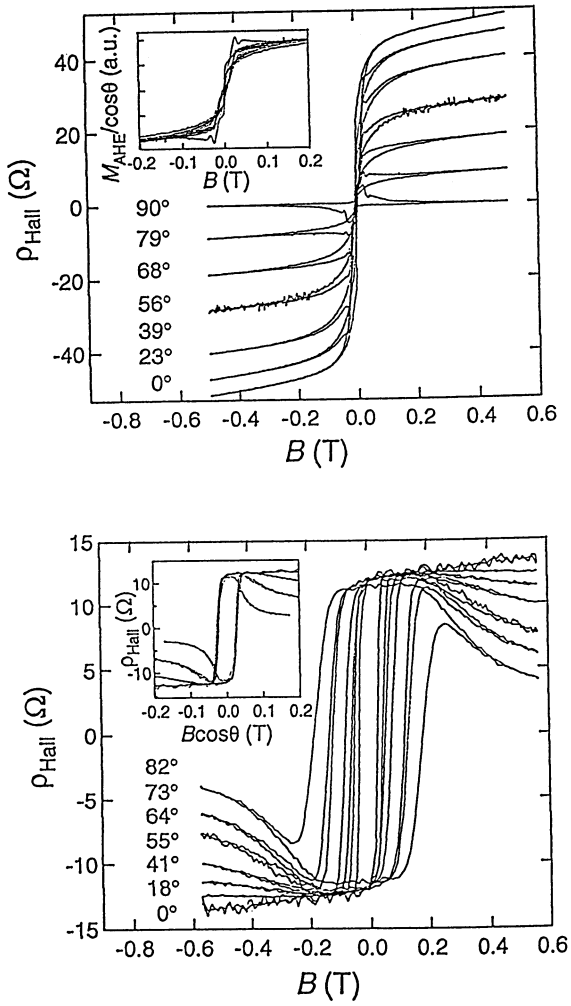

Fig. 6. Hall resistance for different angles of the external magnetic field with respect to the plane normal for samples 1 and 2 in Table 1.

vertical axis. Recalling that the magnetization component perpendicular to the plane is effective to the anomalous Hall effect, this implies that the magnetization vector stays parallel to the external field, indicating very small magnetic anisotropy. In the case of sample 2 (Fig. 6(b)), by contrast, scaling is achieved by taking $B\cos\theta$ as the horizontal axis. This implies that the magnetization vector is always perpendicular to the film plane, and only the normal component of the external field is effective, indicating a strong perpendicular magnetic anisotropy. Such differences in magnetic anisotropy originate from lattice-mismatch-induced strain in the magnetic layer as inferred in earlier study [10]. The present result clearly indicate that the strong perpendicular magnetic anisotropy is caused by tensile stress exerted on the $In_{1-x}Mn_xAs$ layers, which is stronger for AlSb underlayer than for GaSb underlayer. The $In_{1-x}Mn_xAs$ layer of sample 1 is 20 nm thick which appears to be larger than the critical thickness for introduction of dislocations, so that the strain is relaxed to some extent.

Table 1
The parameters of ultrathin film samples of $In_{1-x}Mn_xAs$

Sample	x	d (nm)	Underlayer	Lattice mismatch (%)	T_C (K)
1	0.18	20	$Ga_{0.7}Al_{0.3}Sb$	0.94	~35
2	0.12	9	GaSb	0.70	~35
3	0.12	9	AlSb	1.3	~35

5. Magnetotransport and metal-insulator transition

Fig. 7 shows the longitudinal and Hall resistivities of the metallic $Ga_{1-x}Mn_xAs$ sample ($x = 0.035$). As stated earlier, the Hall resistivity ρ_{xy} in these materials is dominated by the anomalous term so that the $\rho_{xy}(B)$ curve reflects the magnetization curve. While this provides a sensitive built-in probe for the magnetism, this poses a serious difficulty in obtaining information on the carrier density. The standard procedure of extracting the carrier density from the Hall effect cannot be applied straightforwardly. For the metallic sample ($x = 0.035$) shown in Fig. 7, the magnetization quickly reaches the saturation value and is nearly constant in the high field region, as shown in Fig. 4. Therefore, it seems reasonable for this sample to take the slope of the $\rho_{xy}(B)$curve at low temperature and high magnetic field, where the magnetization is saturated. The hole density thus obtained is $p \approx 4 \times 10^{20}$ cm^{-3}. This is roughly half the value calculated by assuming that the Mn ions are in the divalent state and supply a single hole each.

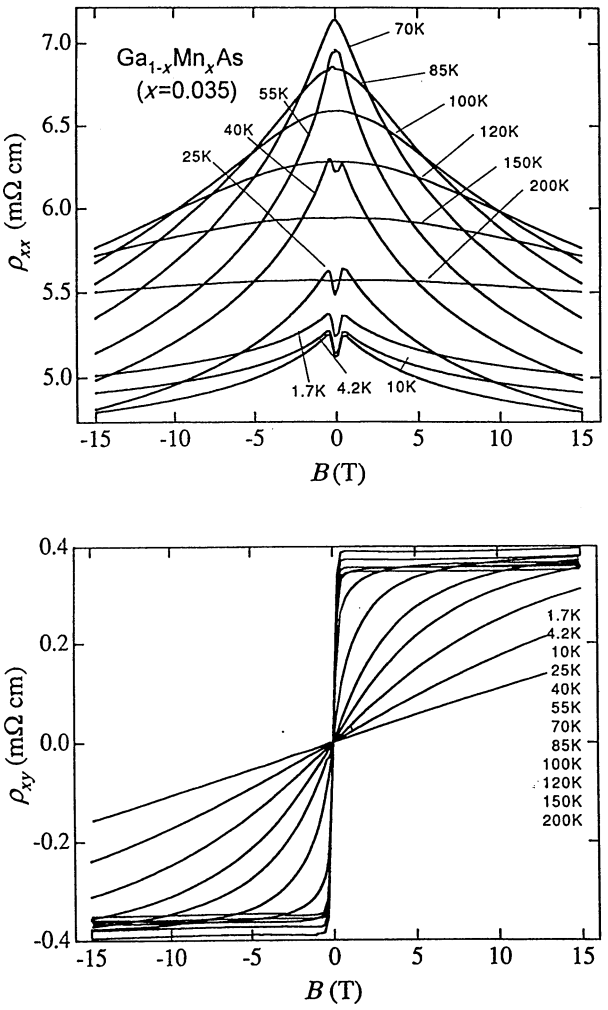

Fig. 7. Longitudinal resistivity ρ_{xx} and Hall resistivity ρ_{xy} in $Ga_{1-x}Mn_xAs$ with $x = 0.035$ at different temperatures.

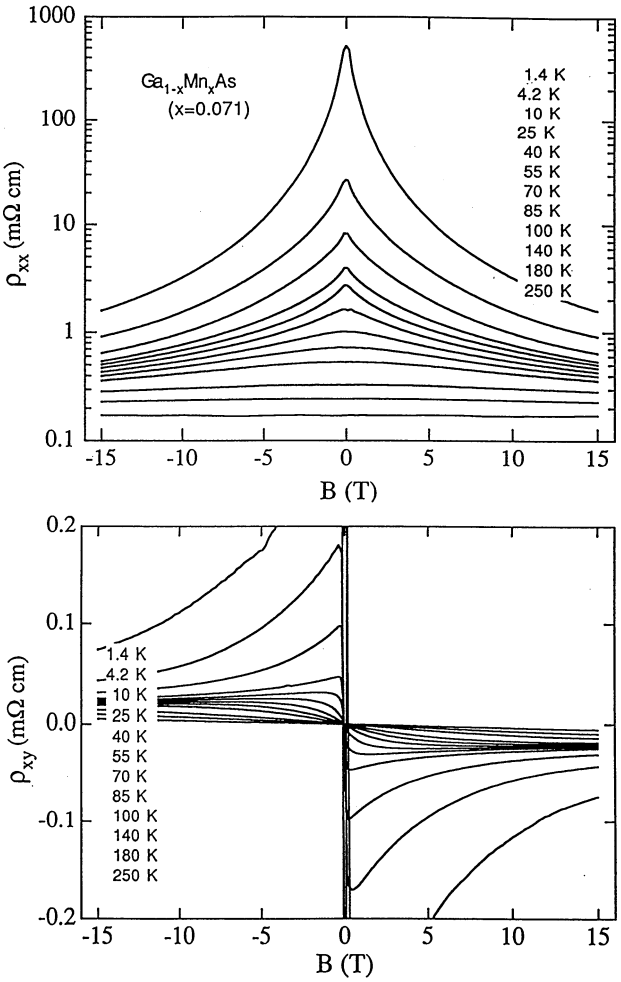

Fig. 8. Longitudinal resistivity ρ_{xx} and Hall resistivity ρ_{xy} in $Ga_{1-x}Mn_xAs$ with $x = 0.071$ at different temperatures.

The longitudinal resistivity ρ_{xx} shows a rather complicated T- and B-dependence. At temperatures below T_C and in the low field range, a small positive magnetoresistance is seen. This positive magnetoresistance is present only in the ferromagnetic phase and is found to be sensitive to the magnetic field orientation with respect to the transport current. It is, therefore, attributed to the so-called anisotropic magnetoresistance effect ubiquitously observed in ferromagnetic materials. Except for this small positive component, the overall magnetoresistance is negative. The negative magnetoresistance becomes largest around T_C. Matsukura et al. [14] analyzed the behavior above and near T_C in terms of the critical spin-disorder scattering model, and obtained the p–d exchange coupling constant $J_{pd} = 150 \pm 40$ eVA^3 which translates to $N_0\beta = 3.5$ eV. This value is somewhat larger than those typically found in II–VI compounds doped with Mn, $N_0\beta \approx 1$–2 eV.

Fig. 8 shows the longitudinal and Hall resistivities of the semiconducting sample on the higher Mn content side ($x = 0.071$). The negative magnetoresistance becomes very large in this semiconducting sample. At the lowest temperature ($T = 1.4$ K), the resistivity in the high field range is diminished by more than two orders of magnitude from the zero-field value. The Hall resistivity shows a very large unusual field dependence. This reflects, through the anomalous Hall coefficient R_s, the large change in the resistivity. Evidently, it is difficult to deduce the magnetization curve from the Hall resistivity data for this sort of samples. This sort of large negative magnetoresistance seems to be a common feature of the semiconducting samples of $Ga_{1-x}Mn_xAs$. Fig. 9 shows the temperature dependence of the resistivity at different magnetic fields. The giant negative magnetoresistance that continues up to high fields is caused by the interaction of hole carriers with localized Mn moments, and it appears to be correlated with the presence of a gradually saturating component of magnetization as seen in Fig. 4.

There are two possible scenarios for the basic mechanism for the large negative magnetoresistance. One is the scenario based on formation of magnetic polaron, i.e. a complex entity consisting of a hole carrier and a cloud of Mn spins partially polarized by the p–d exchange coupling. Such a magnetic polaron tends to be localized in the absence of magnetic field because its motion involves rearrangement of a large number of Mn moments. Application of high magnetic field progressively aligns the Mn moments, and makes the carrier increasingly mobile. This is a scenario proposed earlier for interpretation of the behavior of II–VI compound DMS and $In_{1-x}Mn_xAs$, and may be also applied to the present case of $Ga_{1-x}Mn_xAs$. However, the fact that the large negative magnetoresistance is absent in the $x = 0.015$ sample far from the metal-insulator boundary, seems to favor the second line of interpretation based on Anderson localization.

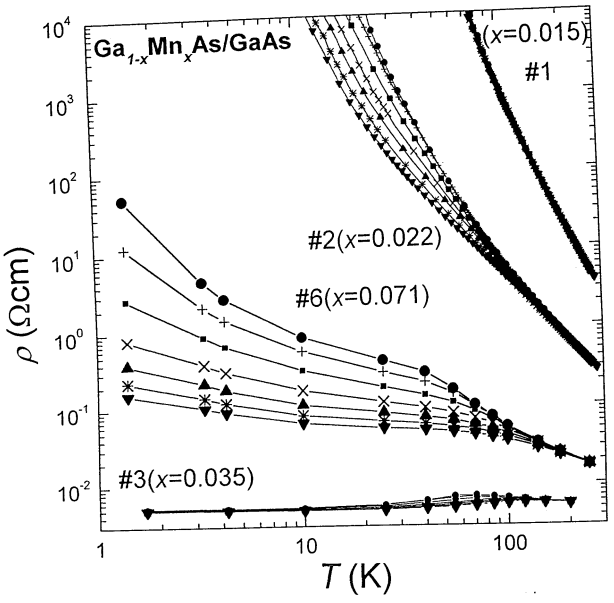

Fig. 9. Temperature dependence of resistivity at different magnetic fields for four samples of $Ga_{1-x}Mn_xAs$.

In a strongly Anderson localized regime, the Fermi energy ε_F lies on the localized side of the mobility edge ε_c. The conductivity at low temperatures is exponentially dependent on the localization length $\xi \propto |\varepsilon_C - \varepsilon_F|^{-\nu}$. The effect of a magnetic field is to cause a Zeeman shift of the Fermi energy by $\pm g\mu H$. This gives rise to a decrease in $|\varepsilon_c - \varepsilon_F|$ for one of the two spin subbands, and causes negative magnetoresistance. This is the scenario first proposed by Fukuyama and Yosida [18] to explain the large negative magnetoresistance found in TaS_2. In the present case of diluted magnetic semiconductors, the Zeeman shift of the Fermi energy $\pm g\mu B$ can be much larger, and the mobility edge may also be shifted as the magnetic field quenches disorder by aligning the Mn moments.

The transport in this sample at temperatures lower than 1 K has turned out to be highly anisotropic within the (100) plane [19]. Fig. 10 shows two sets of data on the same $x = 0.071$ sample for probing current directions along the [01$\bar{1}$]and [011]direction' respectively. As shown in Fig. 10(a), the resistivity in the [01$\bar{1}$] direction obeys the formula for three-dimensional variable range hopping conduction with Coulomb soft gap,

$$\rho(T) = A \exp (T_0/T)^{1/2}. \quad (2)$$

The resistivity in the [011] direction, on the other hand, is lower by one or two orders of magnitude than the [01$\bar{1}$] direction. As shown in Fig. 10(b), the temperature dependence appears to be well represented by

$$\sigma(T) = \sigma(0) + BT^{1/2}, \quad (3)$$

for $T > 0.1$ K. The flattening at the lowest temperature is probably due to some filamentary conducting paths. This result, if taken literally, implies that there is an insulator-to-metal transition at $B \approx 12$ T. This sort of strong in-plane anisotropy is found only in the semiconducting samples on the large x side. The origin of the strong anisotropy is presently unknown, but is presumably associated with anisotropic strain built into the film during the off-equilibrium growth at low temperature, which may result in a highly anisotropic envelope of the localized wavefunction.

6. Conclusion

Study of the III–V compound diluted magnetic semiconductor is a new and rapidly developing field. The exchange coupling between carriers and Mn moments gives rise to interesting magnetic, transport, and optical

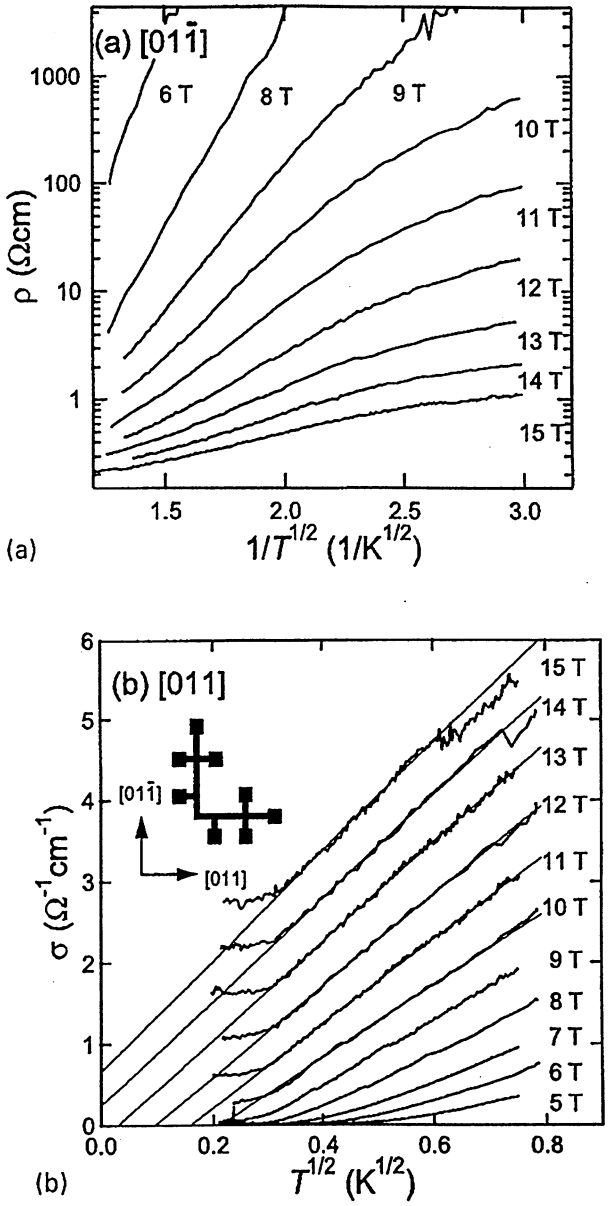

Fig. 10. The anisotropic resistivity of an L-shaped sample of $Ga_{1-x}Mn_xAs$ with $x = 0.071$ at low temperatures: (a) the resistivity along the [01$\bar{1}$] direction plotted as log ρ vs. $T^{-1/2}$; (b) the conductivity along the [011] direction plotted as σ vs. $T^{-1/2}$.

properties. The experimental studies have revealed that the key ingredients governing the magnetic and transport properties are carrier(hole)-mediated ferromagnetic coupling, random distribution and clustering of Mn spins, and lattice-mismatch-induced strain. Although a rough sketch has been drawn, a coherent picture for this class of materials including the mechanism for the occurrence of ferromagnetism is yet to be constructed. We anticipate that the studies of manganites and III–V compound DMS will benefit much from each other.

Acknowledgements

We thank H. Takagi for kindly letting us use his SQUID magnetometer. This work is supported in part by the Grant-in-Aid for Scientific Research for Priority Area 'Spin Controlled Semiconductor Nanostructures' from the Ministry of Education Science Sports and Culture, Japan.

References

[1] See for example, T. Dietl. in: S. Mahajan (Ed.), Handbook on Semiconductors, vol. 3b, chp. 17.
[2] H. Munekata, H. Ohno, S. von Molnar, A. Segmuller, L.L. Chang, L. Esaki, Phys. Rev. Lett. 63 (1989) 1849.
[3] H. Munekata, H. Ohno, R.R. Ruf, R.J. Gambino, L.L. Chang, J. Cryst. Growth 11 (1991) 1011.
[4] H. Ohno, A. Shen, F. Matsukura, A. Oiwa, A. Endo, S. Katsumoto, Y. Iye, Appl. Phys. Lett. 69 (1996) 363.
[5] Y.L. Soo, S.W. Huang, Z.H. Ming, Y.H. Kao, H. Munekata, L.L. Chang, Phys. Rev. B53 (1996) 4905.
[6] R. Shioda, K. Ando, T. Hayashi, M. Tanaka, Phys. Rev. B58 (1998) 1100.
[7] A. Oiwa, S. Katsumoto, A. Endo, M. Hirasawa, Y. Iye, H. Ohno, F. Matsukura, A. Shen, Y. Sugawara, Solid State Commun. 103 (1997) 209.
[8] R.A. Chapman, W.G. Hutchinson, Phys. Rev. Lett. 18 (1967) 443.
[9] D.A. Woodbury, J.S. Blakemore, Phys. Rev. B8 (1973) 3803.
[10] H. Munekata, A. Zaslavsky, P. Fumagalli, R.J. Gambino, Appl. Phys. Lett. 63 (1993) 2929.
[11] Y. Satoh, N. Inoue, Y. Nishikawa, J. Yoshino, Extended Abstract, Third Symposium on the Physics and Application of Spin-Related Phenomena in Semiconductors, November, 1997, Sendai, Japan, p. 23.
[12] H. Munekata, T. Penney, L.L. Chang, Surf. Sci. 267 (1992) 342.
[13] S. Koshihara, A. Oiwa, M. Hirasawa, S. Katsumoto, C. Urano, H. Takagi, H. Munekata, Phys. Rev. Lett. 78 (1997) 4617.
[14] F. Matsukura, A. Shen, H. Ohno, Y. Sugawara, Phys. Rev. B57 (1998) R2037.
[15] H. Akai, Phys. Rev. Lett. 81 (1998) 3002.
[16] A. Oiwa, S. Katsumoto, M. Hirasawa, A. Endo, Y. Iye, H. Munekata, A. Shen, H. Ohno, Extended Abstract, Third Symposium on the Physics and Application of Spin-Related Phenomena in Semiconductors, November, 1997, Sendai, Japan, p. 34.
[17] A. Oiwa, A. Endo, S. Katsumoto, Y. Iye, H. Ohno, H. Munekata, Phys. Rev. B59 (1999) 5826.
[18] H. Fukuyama, K. Yosida, J. Phys. Soc. Jpn. 46 (1979) 102.
[19] A. Oiwa, S. Katsumoto, A. Endo, M. Hirasawa, Y. Iye, F. Matsukura, A. Shen, Y. Sugawara, H. Ohno, Physica B249–251 (1998) 775.